UC Davis
UC Davis Previously Published Works

Title
Cell-secreted extracellular matrix influences cellular composition sequestered from unprocessed bone marrow aspirate for osteogenic grafts

Permalink

Journal

ISSN

Authors
Harvestine, Jenna N
Saiz, Jr., Augustine M
Leach, J Kent

Publication Date
2019-04-23

DOI

Peer reviewed

PAPER

Check for updates

Cell-secreted extracellular matrix influences cellular composition sequestered from unprocessed bone marrow aspirate for osteogenic grafts

Jenna N. Harvestine,[a] Augustine M. Saiz, Jr. [b] and J. Kent Leach [*a,b]

Bone marrow aspirates provide a rich source of cells for use in tissue engineering of bone and other clinical indications. However, progenitor cells such as mesenchymal stem cells (MSCs) account for a small fraction of nucleated cells in bone marrow aspirate (BMA), requiring extensive culture expansion. Accessory cell populations such as endothelial or hematopoietic cells can potentiate the bone-forming potential of MSCs, and cell-secreted extracellular matrix (ECM) can increase cell seeding efficiency and osteogenic differentiation of heterogeneous cell populations. In this study, we hypothesized that cell-secreted ECM could be used to sequester MSCs and accessory cells from BMA for bone regeneration. To generate 3D implantable constructs, BMA was resuspended in media with or without type I collagen or ECM and injected into a perfusion bioreactor system. The addition of protein coatings increased cell seeding efficiency compared to uncoated scaffolds. Compared to fresh BMA, the culture of BMA on all scaffolds reduced the proportion of CD45+ myeloid cells and increased CD31+CD45− endothelial cells. Compared to uncoated scaffolds, we observed a 143- and 30-fold increase in MSCs when fresh BMA was cultured on ECM- or collagen-coated scaffolds, respectively. Upon subcutaneous implantation, ECM-coated scaffolds promoted cell survival and early vascularization. However, bone formation was comparable across all implant groups, suggesting additional osteogenic cues are necessary to increase the bone forming potential of fresh BMA. These results motivate further investigation into strategies which elicit more robust bone regeneration by tissue aspirates.

1. Introduction

Bone marrow aspirate (BMA) represents a clinically accessible source of mesenchymal and hematopoietic stem cells that are under widespread clinical investigation for numerous indications. Bone marrow-derived mesenchymal stem cells (MSCs) are used in orthopaedic applications including bone repair and regeneration due to their multilineage potential and potent secretome containing pro-angiogenic and immunomodulatory factors. However, MSCs represent only 0.01–0.1% of nucleated cells in a BMA,[1] requiring prolonged culture expansion to generate sufficient numbers for clinical procedures. Commercial devices are available to concentrate bone marrow for point-of-care applications, yet there are no reports demonstrating the ability to increase the proportion of MSCs delivered to the patient.[2]

The transplantation of osteogenically induced MSCs is beneficial to drive osteogenesis. However, the simultaneous presentation of microenvironments capable of supporting accessory cells remains a critical challenge in bone tissue engineering. In addition to vascularization, endothelial cells (ECs) and other accessory cells found in tissue aspirates support new bone formation after implantation.[3] We recently reported that heterogeneous populations derived from lipoaspirates demonstrated enhanced osteogenic differentiation with concomitant retention of ECs and CD34+ cells when seeded on cell-secreted ECM.[4] Moreover, this retention occurred over two weeks despite culture in media that tends to select for osteoprogenitor cells and is deleterious to ECs and other cell populations.

Biomaterials designed for bone engineering present structural and biophysical cues to associated cells for osteoconduction, osteoinduction, and integration with the host bone.[5] However, standard clinical practice consists of BMA injection directly into the injured site without a delivery vehicle with anticipation of improved clinical outcomes. The availability of engineered materials capable of enriching the MSC content from BMA would be a critical advancement and valuable tool

aDepartment of Biomedical Engineering, University of California, Davis, Davis, CA 95616, USA. E-mail: jnharvestine@ucdavis.edu, jkleach@ucdavis.edu
bDepartment of Orthopaedic Surgery, School of Medicine, UC Davis Health, Sacramento, CA 95817, USA. E-mail: amsaiz@ucdavis.edu

for bridging defects in bone repair. Furthermore, materials tailored to exploit the regenerative niche of cells in BMA will promote exogenous cell participation and recruit endogenous cells for tissue regeneration.

Highly porous scaffolds that recapitulate native trabecular structure have been manufactured with FDA-approved polymeric and ceramic materials. However, these materials lack the complex organic components of bone extracellular matrix (ECM) that promote bone cell adhesion and function within a heterogeneous niche. ECM provides structural integrity and biochemical cues to instruct tissue-specific cellular function. Decellularized cell-secreted ECM is a naturally derived, complex biomaterial that fulfills these requirements.[6–8] Our group demonstrated the capacity of cell-secreted ECM to increase MSC seeding efficiency onto various platforms including poly-lactide-*co*-glycolide (PLG) and PLG-ceramic composite scaffolds.[9,10] Others reported cell-derived ECM-coated scaffolds improved osteoblastic gene and protein expression by MSCs under perfusion bioreactor culture. Perfusion bioreactors can be used to quickly populate various types of scaffold with cells for direct implantation,[11,12] as a 3D *in vitro* expansion method,[13,14] to maintain a hematopoietic bone marrow niche,[15–17] or to prepare mature osteogenic grafts.[18,19] However, these principles have not yet been combined to prepare osteogenic grafts composed of heterogeneous cell populations from BMA.

We hypothesized that cell-secreted ECM would sequester relevant cells from BMA, support cell survival, and promote osteogenic differentiation of cells upon implantation. To investigate this hypothesis, we assessed the ability of uncoated and protein-coated scaffolds to concentrate MSCs from unprocessed BMA when seeded in a perfusion bioreactor system. We evaluated the resultant composition and the ability of each substrate to prompt tissue infiltration and bone formation in an ectopic site. The results of this study demonstrate the ability of cell-secreted ECM to serve as an effective biomaterial to enrich the MSC population from unprocessed bone marrow aspirates.

2. Materials and methods

ECM production

Human bone marrow-derived MSCs (Lonza, Walkersville, MD) were used without further characterization. MSCs were expanded under standard conditions until use at passages 4–6 in minimum essential alpha medium (α-MEM; w/L-glutamine, w/o ribo/deoxyribonucleosides (Invitrogen, Carlsbad, CA)) supplemented with 10% fetal bovine serum (FBS; Atlanta Biologicals, Flowery Branch, GA) and 1% penicillin (10 000 U mL^{-1}) and streptomycin (10 mg mL^{-1}, Mediatech, Manassas, VA) (P/S). Cell-secreted ECMs were prepared as we described.[9,10,20–22] Briefly, MSCs were seeded at 50 000 cells per cm^2 and cultured in media supplemented with 50 μg mL^{-1} ascorbate 2-phosphate for 10 days with media changes every 2–3 days. After culture, monolayers were washed with phos-

phate buffered saline (PBS) and cells were removed using a detergent-based solution followed by DNase (Sigma, St Louis, MO) treatment (37 °C for 1 h) to remove 99.9% of DNA content from culture post-decellularization.[21] Decellularized ECM was washed 3× with PBS and mechanically dislodged from culture flasks using a cell scraper. Total protein within the collected ECM was quantified using a bicinchoninic acid (BCA) protein assay (Thermo Fisher, Rockford, IL). ECM solutions were frozen in 0.02 N acetic acid at −20 °C until use.

Composite scaffold fabrication

Scaffolds were fabricated using a gas foaming/particulate leaching method as described.[18,23] Microspheres composed of PLG (85 : 15, DLG 7E; Lakeshore Biomaterials, Birmingham, AL) were prepared using a double-emulsion process and lyophilized to form a free-flowing powder. 9.2 mg of lyophilized microspheres were combined with 23.1 mg of hydroxyapatite (HA) crystals (particle size 100 nm, Berkeley Advanced Biomaterials, Berkeley, CA) and 175.6 mg of NaCl (300–500 μm in diameter) to yield a 2.5 : 1 : 19 mass ratio of ceramic : polymer : salt. The powdered mixture was compressed under 2 metric tons for 1 min to form solid disks (final dimensions: 8 mm in diameter and 2 mm in height) using a Carver Press (Carver, Inc., Wabash, IN). Compressed disks were exposed to high pressure CO$_2$ gas (5.5 MPa) for at least 16 h followed by rapid pressure release to prompt polymer fusion. Salt particles were leached from scaffolds in distilled H$_2$O for 24 h to generate HA-PLG composite scaffolds. Scaffolds were sterilized by 70% ethanol under gentle vacuum followed by two rinses in sterile PBS.

Seeding bone marrow aspirate in perfusion bioreactors

Unprocessed human bone marrow aspirate (BMA) was from Lonza (10 mL of aspirate from $n = 2$ male and $n = 2$ female donors; 23–32 years old, mean age 26 ± 4 years). BMA was diluted 1 : 5 in PBS and pelleted by centrifugation at 1000g. Cells were incubated in a red blood cell lysis buffer (154.4 mM ammonium chloride, 10 mM potassium bicarbonate, and 97.3 mM EDTA tetrasodium salt)[24] for 5 min at 37 °C, washed with PBS, and viable cells were quantified using a Countess® II Automated Cell Counter (Thermo Fisher). Culture media was composed in equal parts of α-MEM supplemented with 10% FBS and 1% P/S, EGM-2 MV, and RPMI supplemented with 10% FBS and 1% P/S. Bioreactor seeding was performed as previously described.[18,25] Briefly, scaffolds were installed into U-CUP flow perfusion bioreactors (Cellec Biotek, Basel, Switzerland), and 10 mL of co-culture medium was injected into the bottom port. Remaining media was further supplemented with 100 μg mL^{-1} of collagen or ECM to produce protein-coated scaffolds (Fig. 1A). Cells were resuspended in media with or without protein and 2 mL of solution was injected as described (Fig. 1B). Bioreactors were perfused at a superficial velocity of 3 mL min^{-1} for 20 h to seed the constructs (Fig. 1C).
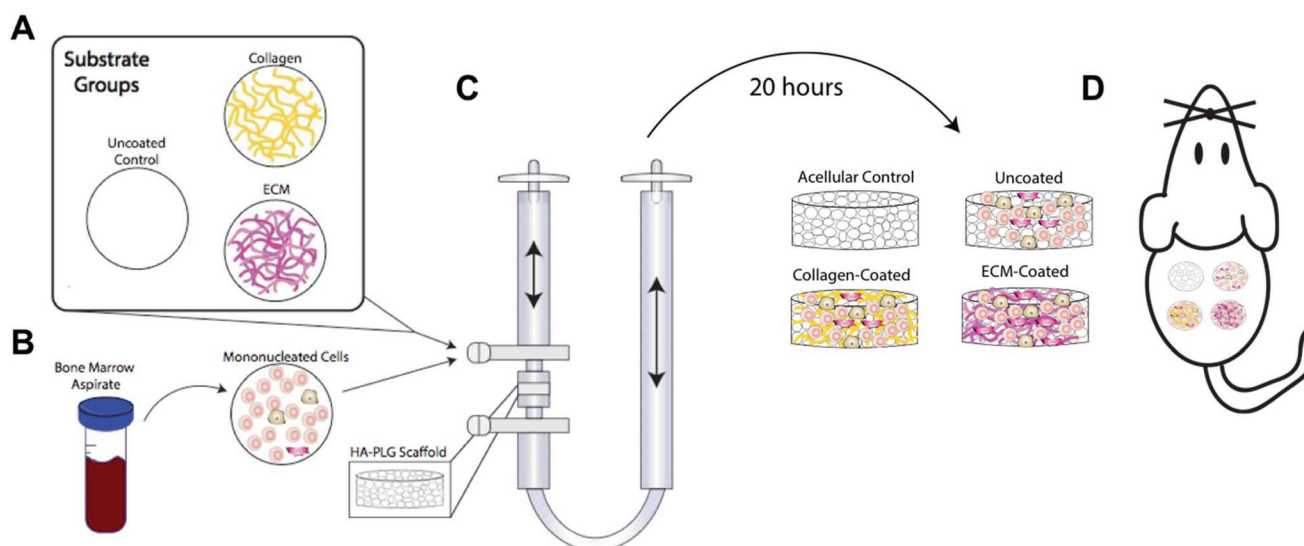
Fig. 1 Schematic of experimental design. (A) Control media or media containing equal quantities of collagen or cell-secreted extracellular matrix (ECM) were mixed with (B) mononucleated cells from BMA and injected into (C) perfusion bioreactors containing HA-PLG scaffolds press-fit into the perfusion chamber. After 20 hours of oscillating perfusion, scaffolds were retrieved and (D) implanted into subcutaneous pockets in the back of nude rats.

BMA seeding efficiency and immunophenotype of entrapped cells

To determine the number of entrapped cells, DNA content of unentrapped cells was compared to known quantities of cells from unseeded BMA using a Quant-iT PicoGreen dsDNA Assay Kit (Invitrogen) and subtracted from the number of cells seeded. Entrapped cells were liberated from scaffolds through enzymatic and mechanical digestion. The immunophenotype of retrieved cells was determined using flow cytometry. Briefly, non-specific binding was blocked by incubation in Protein Block (AB156024, Abcam, Cambridge, MA) for 20 min and then incubated with antibodies against CD31 (303110), CD45 (368518), CD34 (343623), CD90 (328112), and CD73 (344008) (all from BioLegend, San Diego, CA) per manufacturer's instructions.

Histological analysis and scanning electron microscopy

Scaffolds were fixed in 10% formalin acetate overnight at 4 °C, washed 2× with water, soaked overnight in OCT compound, frozen, and sectioned at 5 μm. Cell distribution throughout the scaffold was visualized using a DAPI nuclear stain (D1306, Invitrogen).

Pore architecture and protein adsorption to the pore surface were visualized with scanning electron microscopy.[9,18] Scaffolds were fixed in freshly prepared Karnovsky's fixative solution overnight at 4 °C, washed 2× with water, bisected, and dehydrated in increasing concentrations of ethanol. Following dehydration, samples were critical point dried (Supercritical AutoSamdri-931, Tousimis Research Corp, Rockville, MD), fixed to stubs with silver paste, sputter coated with gold (Pelco SC-7 Auto Sputter Coater), and imaged using a scanning electron microscope (Quattro ESEM, Thermo Fisher, Newington, NH).

Subcutaneous implantation

All animal procedures were performed in accordance with the Guidelines for Care and Use of Laboratory Animals of the National Institutes of Health and UC Davis, and experiments were approved by the Animal Ethics Committee of UC Davis. Male 7-week-old nude rats (Taconic Biosciences, Germantown, NY) were anesthetized (3.0%) and maintained (1.5%) under an isoflurane/O_2 mixture delivered through a nose cone at 6 L min^{-1}. Implants were seeded in the bioreactor for 20 hours and bisected prior to implantation. Each animal received four randomized subcutaneous implants: acellular scaffold, uncoated scaffold, collagen-coated scaffold, and ECM-coated scaffold (Fig. 1D). Animals were euthanized at 10, 24, or 42 days post-implantation, and scaffolds were collected and fixed in 10% buffered formalin acetate for 1 day at 4 °C. Samples were washed 2× in PBS to remove residual formalin acetate and preserved in 70% ethanol at 4 °C until further processing.

Qualitative and quantitative three-dimensional analysis of explants at 42 days were conducted using microCT.[18,22] Explants were imaged (55 kVp, 145 mA, 300 ms integration time, average of 3 images) using a high-resolution microCT specimen scanner (mCT 35, Scanco Medical; Brüttisellen, Switzerland). Contiguous slices of 2048 × 2048 pixels were imaged with 12 μm resolution and slice thickness (voxels). Serial tomograms were reconstructed from raw data of 1000 projections per 180° using a cone beam filtered back projection algorithm.[26] The tomograms were calibrated to 0.0, 99.6, 200.0, 401.0 and 800.3 mg HA per cm^3 concentrations of HA so that grey-values of the images were converted to units of density in mg HA per cm^3. The entire scaffold was analyzed by contouring to its edges based on a threshold of 256 mg HA per cm^3. Material in the reconstructed images was partitioned by a

threshold of 256–3000 mg HA per cm^3 to discriminate between mineralized and unmineralized tissue. After thresholding, the image noise was reduced using a low pass Gaussian filter (σ = 0.8, support = 1). Bone volume fraction (BV/TV) was determined by dividing the number of pixels representing bone tissue (BV: bone volume) by the number of pixels in the cylindrical segment (TV: total volume).

After microCT analysis, explants were demineralized in Calci-clear (National Diagnostics, Atlanta, GA) for 24 h, washed 2× in PBS, dehydrated, paraffin-embedded, and sectioned at 5 μm thickness. To visualize tissue formation and morphology, sections were stained with hematoxylin and eosin (H&E) and Masson's trichrome. Blood vessel density at 10 days was quantified using H&E stained cross-sections and consisted of counting circular structures with well-defined lumens. To detect the persistence of human cells, sections were immunostained with a primary antibody against human mitochondria (1:200, AB92824, Abcam).[27]

Statistical analysis

Data are presented as means ± standard deviation of n = 3–6 replicates from 2–3 biological donors unless otherwise stated. Statistical analyses were performed with two-way ANOVA, followed by Tukey's multiple comparison *post hoc* test (GraphPad Prism 7.0, San Diego, CA) to determine significance ($p < 0.05$). Significance is denoted by alphabetical letterings; groups with no significance are linked by the same letters, while groups with significance do not share a letter. A lack of significance between groups is indicated with "ns" and a line bridging non-significant groups.

3. Results

Protein coatings enhance cell entrapment

Scaffolds were perfused with increasing numbers of cells from the BMA over the 20 h seeding duration (Fig. 2A) to determine an effective seeding density. The perfusion of 7.5×10^6 cells resulted in 2.0×10^6 cells entrapped within the scaffold, equivalent to 20×10^6 cells per mL of implantable material. Therefore, 7.5×10^6 cells were used for all subsequent experiments. Compared to uncoated scaffolds, the number of entrapped cells increased by 5.0- and 2.2-fold in collagen-coated and ECM-coated scaffolds, respectively (Fig. 2B). Scanning electron microscopy (SEM) revealed the topography and gross pore structure of uncoated and protein-coated scaffolds (Fig. 2C). No appreciable differences in pore morphology were visible with the introduction of protein coatings (Fig. 2C, top row). In uncoated and collagen-coated scaffolds, cells appeared rounded and grouped in clusters on the surface of pores. In addition to rounded cells, we observed a stretched, spindle-like morphology for some cells on ECM-coated scaffolds, indicative of successfully entrapping a heterogeneous population of non-adherent and anchorage-dependent cells (Fig. 2C, bottom row). Picrosirius red staining revealed collagen-coating was isolated to the pore surfaces,

whereas ECM coating was apparent on pore surfaces and throughout the pore volume (Fig. 2D). We observed uniform cell distribution in all scaffolds, regardless of coating (Fig. 2E), and we did not detect differences in cell adhesion as a function of donor gender.

Cell-secreted ECM concentrates MSCs from BMA

We used flow cytometry to determine the immunophenotype of cells before and after seeding onto scaffolds (Fig. 3A). Myeloid cells, a heterogeneous population of hematopoietic cell lineages identified as CD45+, constituted 85% of cells in fresh BMA. After seeding, the overall proportion of CD45+ was significantly reduced to between 49–58% in all substrates (Fig. 3B). However, the proportion of hematopoietic progenitor cells, identified as CD45+CD34+, entrapped within all substrates remained similar to fresh aspirate (Fig. 3C). Less than 15% of cells in the fresh BMA were identified as endothelial cells, CD31+CD45−. After seeding, this proportion was significantly increased in all substrates (Fig. 3D). As expected, less than 0.1% of BMA was CD73+CD90+CD45−, representing the MSCs. The proportion of MSCs increased 30- and 143-fold to 2.6% ± 1.3% of entrapped cells in collagen-coated scaffolds and ECM-coated scaffolds, respectively (Fig. 3E).

ECM-coated scaffolds increase vessel formation

To investigate substrate-specific tissue formation, scaffolds were seeded for 20 hours, bisected, and implanted subcutaneously in the back of nude rats. Each rat received 4 randomly arranged implants: an uncoated acellular scaffold and three cellular scaffolds that were uncoated, collagen-coated, or ECM-coated. After 10 days, three rats were collected to evaluate cellular content, tissue formation, and vessel density. While all grafts maintained their overall morphology, collagen-coated scaffolds exhibited significant degradation when comparing the thickness to the acellular and uncoated grafts, manifesting in an overall reduction in the cross-sectional area (Fig. 4A). Hematoxylin and eosin staining (Fig. 4D) revealed robust, uniform, cellular infiltration in all substrates. Despite similar cellularity within grafts (Fig. 4B) the presence of protein coatings elicited greater vascular infiltration, with the greatest vessel density observed in ECM-coated scaffolds (Fig. 4C). All groups displayed early collagen deposition (blue staining) intermixed with non-collagenous matrix deposition (red staining) (Fig. 4E). Despite similar total cellularity, only collagen- and ECM-coated scaffolds demonstrated appreciable persistence of human cells 10 days after implantation (Fig. 4F, top row). After 3 weeks, human cells were only detected on ECM-coated scaffolds (Fig. 4F, bottom row).

ECM-coated scaffolds result in comparable bone formation at 6 weeks

All remaining scaffolds were collected after 6 weeks of ectopic implantation and analyzed for bone and tissue formation. Penetrating vasculature and tissue infiltration were evident to the naked eye upon tissue explant (Fig. 5A). Microcomputed tomography (μCT) revealed similar bone volume fraction
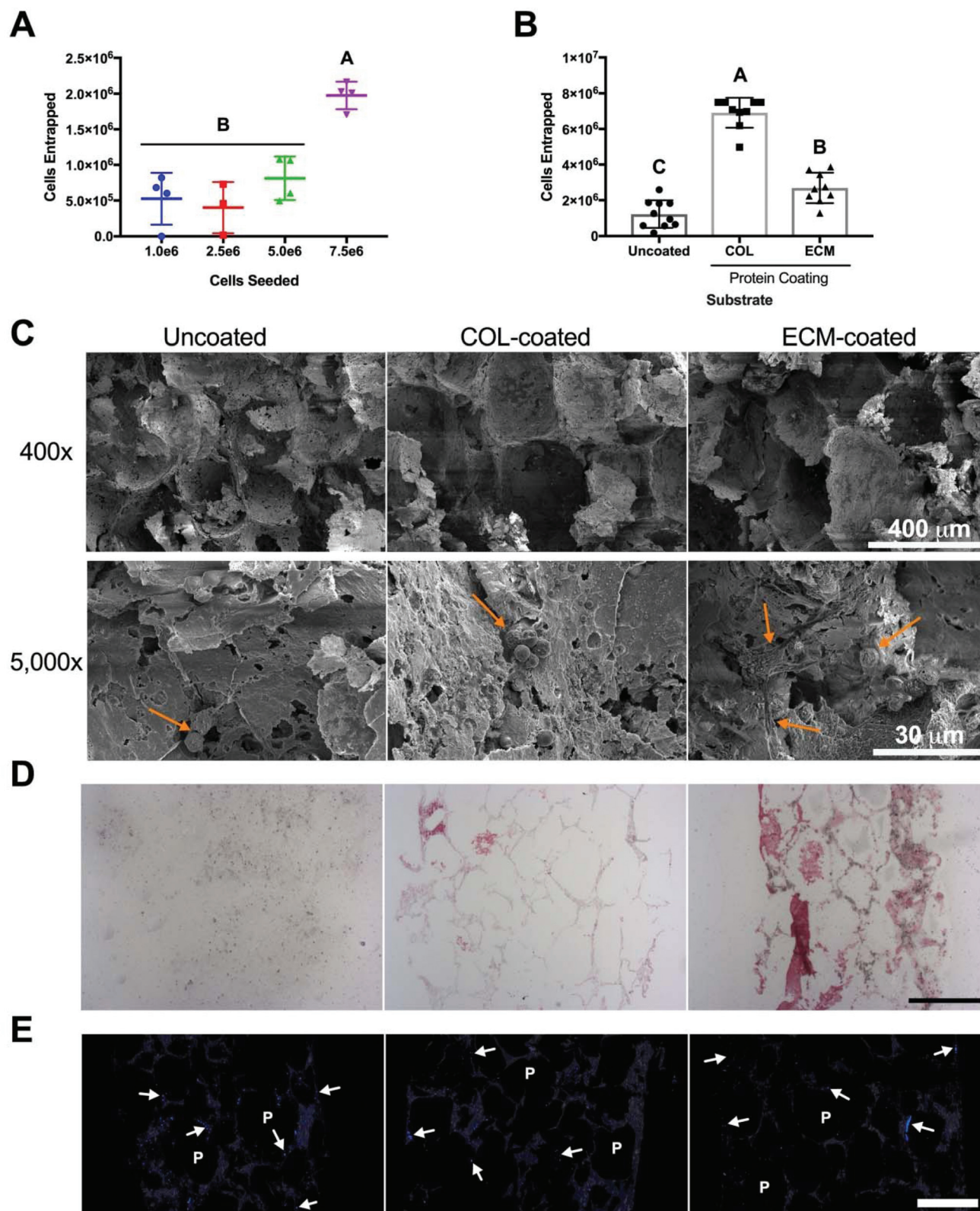
Fig. 2 Bone marrow aspirate is entrapped and homogeneously distributed *via* perfusion culture. (A) Cells entrapped as a function of the number of cells seeded ($n = 4$ replicates from 1 biological donor). (B) Number of cells entrapped per scaffold when seeding 7.5×10^6 cells ($n = 4$ replicates each from 2 biological donors). (C) SEM images of (top) acellular scaffolds (400× magnification) and (bottom) cellular scaffolds (5000× magnification). Orange arrows denote entrapped cells. Scale bars are (top) 400 µm and (bottom) 30 µm. (D) Histological sections stained with picrosirius red reveal collagen distribution; scale bar is 500 µm. (E) DAPI-stained sections confirm homogeneous cell distribution (denoted by white arrows) throughout scaffold pores (denoted by P); scale bar is 500 µm.
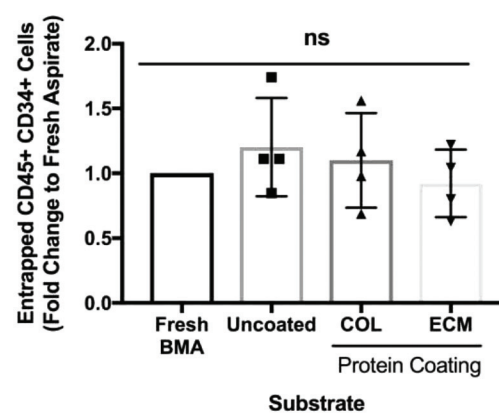
A

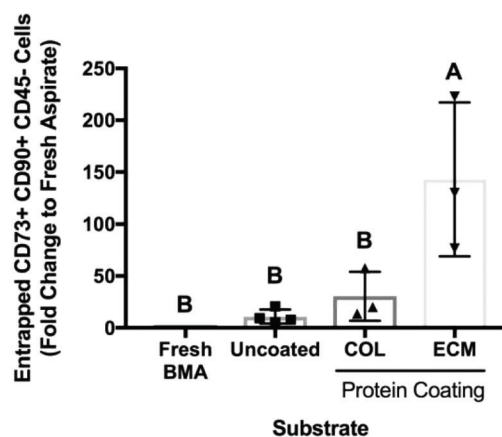| Cell Type	CD Markers	Fresh Isolate	Uncoated	Collagen-Coated	ECM-Coated
Myeloid Cell	CD45+	85.2 ± 1.1%	58.4 ± 5.5%	52.1 ± 7.9%	49.16 ± 4.6%
Myeloid Progenitor	CD45+ CD34+	8.89 ± 0.1%	10.7 ± 3.4%	9.8 ± 3.2%	8.2 ± 2.3%
Endothelial Cell	CD31+ CD45-	13.6 ± 0.6%	22.1 ± 2.3%	21.7 ± 3.4%	20.5 ± 4.5%
Endothelial Progenitor	CD31+ CD34+ CD45-	4.6 ± 0.5%	8.36 ± 0.5%	7.7 ± 1.6%	6.8 ± 2.1%
Mesenchymal Stem Cell	CD73+ CD90+ CD45-	0.02 ± 0.002%	0.19 ± 0.1%	1.0 ± 0.9%	2.6 ± 1.3%
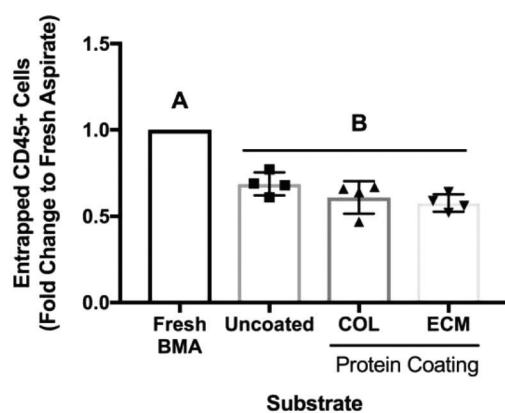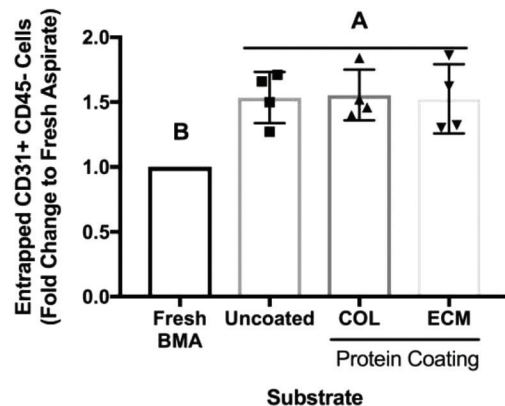
Fig. 3 Immunophenotype of fresh and entrapped BMA. (A) Immunophenotype of unprocessed BMA and cells entrapped in scaffolds. (B–E) Percentage of entrapped cells that are (B) hematopoietic cells (CD45+), (C) hematopoietic progenitor cells (CD45+CD34+), (D) endothelial cells (CD31+CD45−), and (E) mesenchymal stem cells (CD73+CD90+CD45−) shown as a fold change to the percentage found in fresh BMA ($n = 4$ replicates from 1 biological donor).
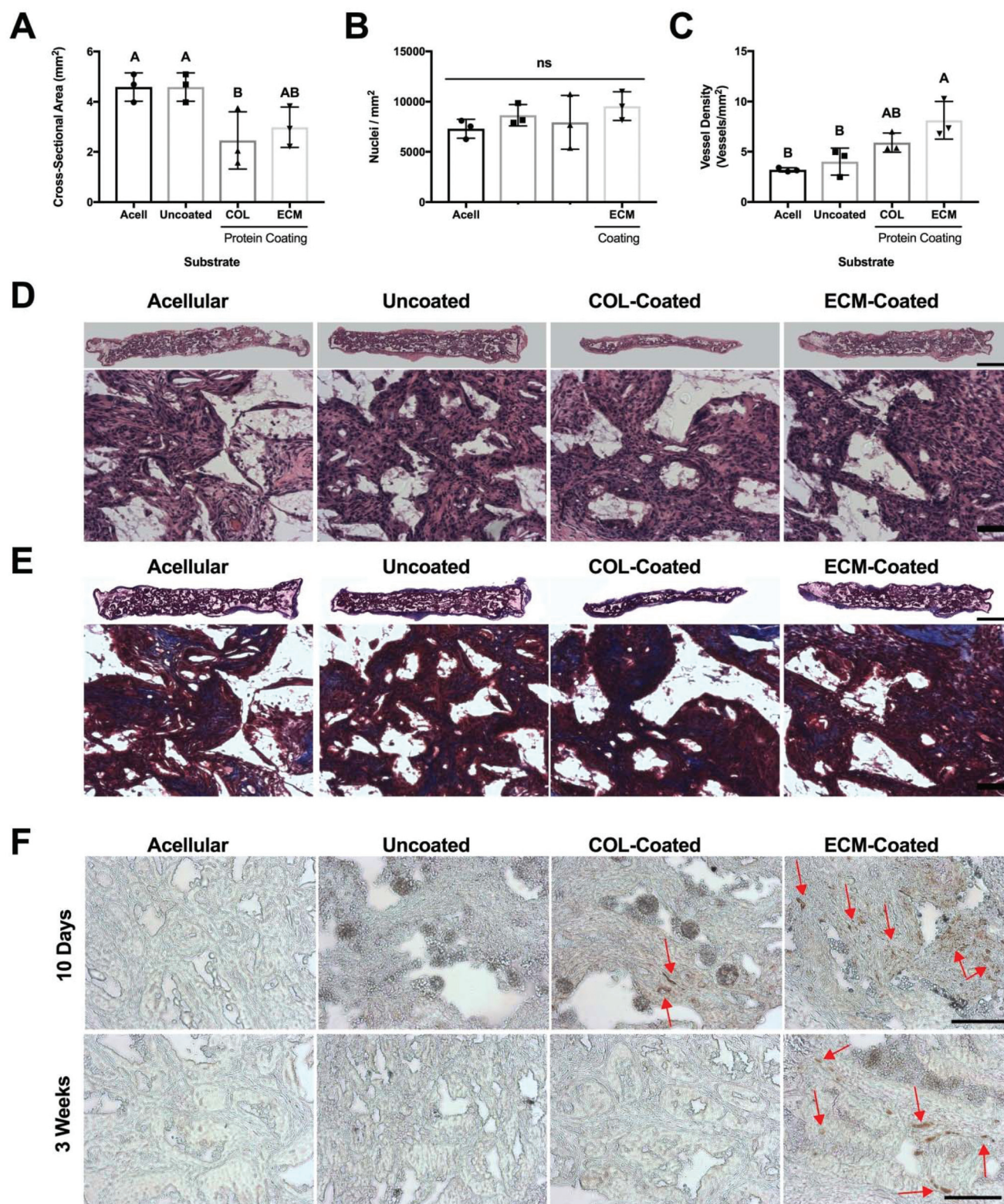
Fig. 4 Analysis of explants after 10 days of subcutaneous implantation. (A) Scaffold cross-sectional surface area. (B) Scaffold cellularity (nuclei per mm²). (C) Quantification of vessel density (A−C quantified from n = 3 slides each from 3 animals). (D−E) Representative images of slides stained for (D) hematoxylin and eosin and (E) Masson's trichrome. Images showing entire cross section (scale bar represents 1 mm) are located above 20× magnification images (scale bar represents 50 μm). (F) Immunostaining for the detection of human cells (denoted by red arrows) after (top row) 10 days and (bottom row) 3 weeks using human-specific anti-mitochondria antibody. Scale bar represents 100 μm.
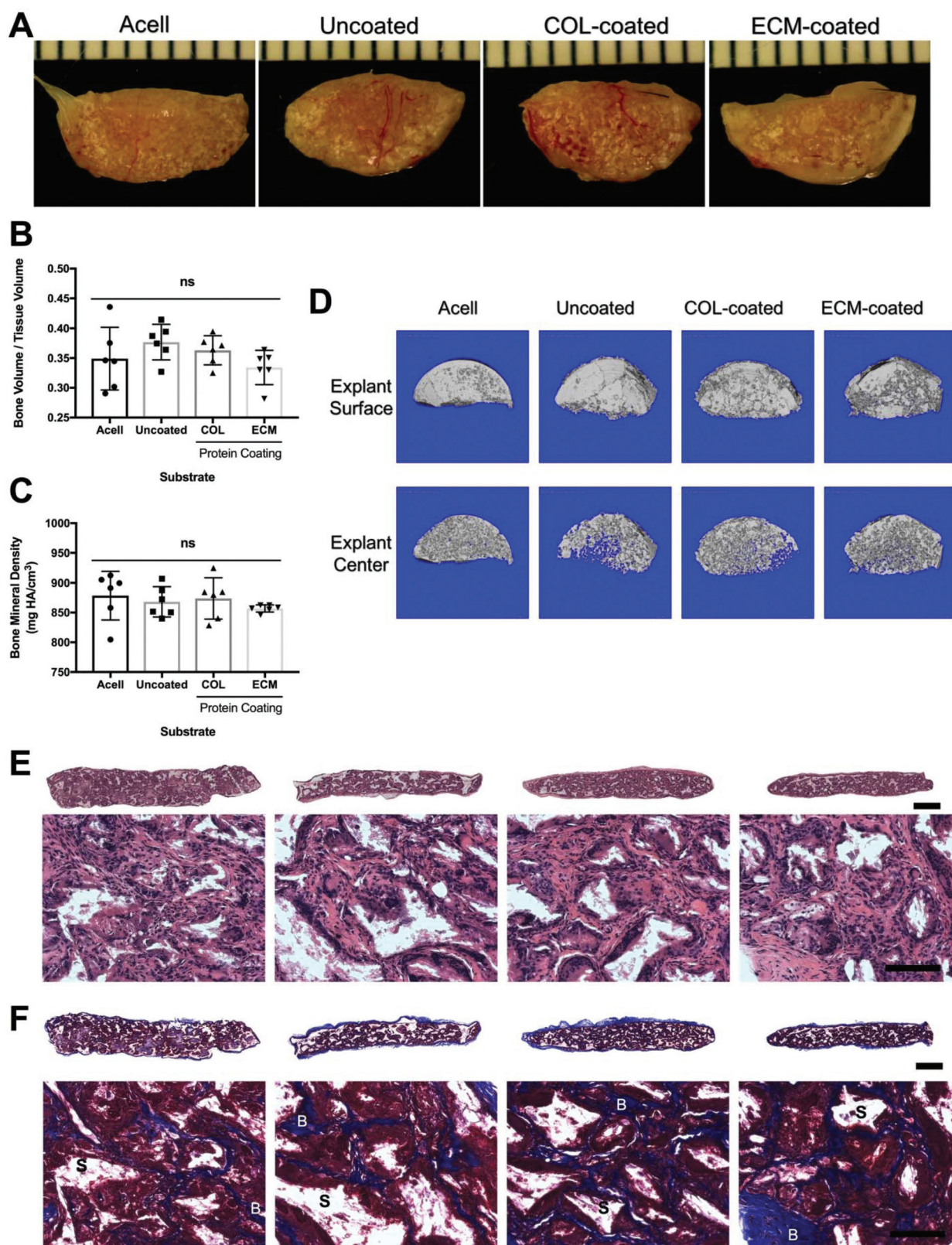
Fig. 5 Assessment of bone formation after 6 weeks. (A) Representative images of explant. (B) Bone volume fraction. (C) Bone mineral density. (D) Representative μCT images at the surface (top row) and center (bottom row) of explants at 6 weeks post-implantation. (E–F) Representative images of slides stained for (E) hematoxylin and eosin and (F) Masson's trichrome. Scale bar represents (top) 1 mm for whole tissue sections and (bottom) 500 μm in 20× images. Scaffold is denoted "S" and new bone "B".

(Fig. 5B) and bone mineral density (Fig. 5C) in all groups. The quantitative data were confirmed *via* reconstructed µCT images of each explant (Fig. 5D). All scaffolds exhibited robust bone formation around the peripheral surface of the scaffold as well as throughout the central regions, demonstrating uniform bone formation throughout the tissue volume. H&E staining further revealed uniform tissue formation, areas of new bone formation (denoted as B) and residual scaffold material (denoted as S) (Fig. 5E). Masson's trichrome staining showed distinct networks of collagen deposition throughout the scaffold cross-section (Fig. 5F).

4. Discussion

The clinical effectiveness of autografts for bone repair is linked to the complex milieu of organic and inorganic components present in native bone, which provide physical and biochemical cues to promote bone regeneration. Motivated by the therapeutic potential of this heterogeneous cell composition, minimally processed aspirates from bone marrow and adipose tissue are under investigation to promote neovascularization and tissue repair.[11,12,28] Once transplanted, however, these cells lack sufficient instructive cues and supportive structure for survival, localization, and activation at the target site. To recapitulate this niche, we fabricated macroporous, composite scaffolds formed of FDA-approved polymers and bioceramics, together with cell-secreted ECM,[9,10,20–22] to provide instructive cues and sequester a complex mixture of cells for tissue formation. We recently reported that this ECM was more effective in retaining accessory cells from lipoaspirates and promoting osteogenic differentiation compared to collagen, a predominant ECM protein found in bone tissue.[4] In these studies, we investigated if this matrix would be sufficient to elicit an osteogenic response from this cell population without additional osteogenic cues. Therefore, we provided minimal *in vitro* osteogenic priming and evaluated bone formation following subcutaneous implantation.

3D perfusion culture increases matrix deposition by stromal cells[29] and *in situ* presentation of stromal and osteoblastic cell-derived ECM has been used to generate a hematopoietic niche capable of supporting CD34+ hematopoietic stem and progenitor cells (HSPCs) under perfusion culture.[17] Others used a perfusion system to expand the MSC population directly from bone marrow aspirates and observed greater *in vivo* bone formation on perfused ceramic constructs compared to cells expanded in monolayer culture.[13] In this study, mononucleated cells from BMA were loaded into perfusion bioreactors alone or mixed with collagen or cell-secreted ECM to populate scaffolds with cells and extracellular proteins simultaneously. Compared to uncoated scaffolds, protein-coated scaffolds increased seeding efficiency of cells. This study was limited to specific parameters and sought to advance previous work by our group and others that have examined experimental parameters such as flow rate and perfusion time.[18] We selected 100 µg mL^{-1} (2 µg ECM per µL scaffold volume) based on our

previous findings that established ECM concentrations of at least 1.17 µg ECM per µL scaffold volume promoted maximal MSC adhesion and osteogenic response.[9] Using perfusion coating, we were able to coat scaffolds at higher concentrations to promote continued bioactivity. The proportion of endothelial cells was increased in all scaffold substrates after seeding, yet only ECM-coated scaffolds were able to increase the proportion of sequestered MSCs (143-fold increase from fresh BMA). Due to the short time in culture, the significant increase in the proportion of MSCs present is likely a result of cell–ligand interactions made available by the diverse protein content of cell secreted ECM,[4,7] rather than cell proliferation. In agreement with previous studies,[9,10,22] ECM-coatings prolonged implanted cell survival, promoted greater tissue formation, and increased vessel density. Despite these early advantages, we observed similar bone formation for all substrates over 6 weeks, evidenced by uniform mineral deposition throughout the construct volume.

Ectopic models of bone formation are an important test of a construct's osteogenic capacity, as there are limited osteoinductive cues presented to the material from endogenous sources. In previous *in vitro* studies, we reported a synergy for MSCs seeded on ECM-coated substrates in the presence of soluble osteogenic cues.[4,10] However, this effect was not perpetuated upon ectopic implantation where endogenous osteogenic signaling is lacking.[10] Previous reports on tissue aspirates describe benefits of *in vitro* preconditioning towards a desired phenotype to achieve enhanced tissue regeneration.[28] However, a shorter culture duration would strengthen the clinical translation for autologous cell therapies. In this study, cells underwent minimal *ex vivo* culture prior to implantation. While the osteoconductive nature of hydroxyapatite prompted bone formation within all scaffolds, the lack of osteogenic phenotype of implanted cells may have limited their effectiveness or any advantages over an acellular scaffold. These findings suggest that investigation of this construct in an orthotopic defect presenting endogenous osteoinductive cues is warranted to determine the effectiveness of this approach.

Perfusion bioreactor culture is amenable to automated controls, lessening the hurdle to process tissue aspirates under Good Manufacturing Practices standards. However, constructs must be sized to fit the dimensions of the unit in order to facilitate uniform and effective perfusion. This limits customization to patient-specific anatomy or results in production of larger constructs with volumes that will be discarded, necessitating the capability for easy manipulation of these materials using tools readily available in the operating theatre. Pure ceramic implants are osteoconductive yet brittle; however, the addition of polymeric components reduces the handling burden, making them more easily tailored to fit a unique defect. In this study, protein-coatings were applied simultaneously during cell seeding, but we recognize the advantageous nature and adaptability of this system to prepare scaffolds for off-the-shelf use. Of particular interest for bone tissue engineering, the fluid shear stress generated during perfusion culture induces an osteogenic phenotype in bone and

bone progenitor cells.[19,30] Similar to phenotype regression after the removal of soluble cues,[22] signaling *via* mechanotransduction from short-term exposure and removal of mechanical stimuli may be quickly lost. In this study, we cultured BMA under perfusion for only 20 hours and then implanted the resultant construct. Although MSCs constituted 2% or less of implanted cells, we observed similar bone volume fraction to a previous study in the laboratory when expanded MSCs—representing 50-fold more MSCs compared to this study—were seeded into the same composite scaffold for 1 day of perfusion culture.[18] In that study, greater bone formation was achieved when cells were exposed to osteogenic perfusion culture for two weeks prior to implantation.[18] Others reported the beneficial effect that 3-dimensional (3D) expansion of BMA prior to implantation has on the bone forming potential *in vivo*.[13] Collectively, the results suggest a robust osteogenic response may require either a greater number of cells to be implanted and/or osteogenic preconditioning of cells prior to implantation. However, there is no direct comparison in bone formation by 3D expanded BMA *versus* its freshly isolated counterpart. This approach merits further investigation to determine if an *in vitro* expansion of autologous cells is beneficial, or necessary, for robust bone formation. Furthermore, this study was limited to a single flow rate, perfusion duration, and ECM concentration. The investigation into additional parameters may provide an improved understanding of how preconditioning parameters effect the bone forming potential of BMA.

In these studies, we employed a short *in vitro* seeding period to model the collection of BMA one day prior to surgical intervention and successfully increased the proportion of entrapped MSCs on ECM-coated scaffolds. Clinical outcomes demonstrate a positive correlation between the number of colony forming units and bone formation by autologous BMA injection.[31] Yet, MSCs represent less than 0.1% of cells from BMA and become further diluted in large aspiration volumes. The capacity to predict or establish uniform consistency with this approach is limited by other variables such as site of aspiration, volume collected, and donor-to-donor variability. Current technologies concentrate aspirates but lack the ability to select for the MSC population.[2] Using a material such as cell-secreted ECM to enhance the MSC population from BMA would alleviate concerns about diluting potent cell populations when large aspirate volumes are needed in clinical practice. Herein, we observed increases in the MSC population when seeded on MSC-secreted ECM compared to endothelial cells, which were increased similarly on all substrates. While we did not extensively test for other adherent cell types, the use of cell- or tissue-specific ECM to concentrate target cell types may present unique advantages for other applications and merits further investigation.

5. Conclusion

These results demonstrate that cell-secreted ECM can select MSCs from BMA and effectively concentrate both MSCs and endothelial cells into an implantable graft. Although we observed improved vascularization and cell survival on ECM-coated scaffolds, these advantages did not translate to increased bone formation in an ectopic site. These data suggest that osteoinductive cues may be necessary to elicit a stronger osteogenic phenotype within fresh BMA. Therefore, future research employing an extended culture duration to induce an osteogenic phenotype or the inclusion of potent osteoinductive cues may be necessary to increase the bone forming potential of a BMA.

Conflicts of interest

There are no conflicts of interest to declare.

Acknowledgements

References

1 M. Alvarez-Viejo, Y. Menendez-Menendez, M. A. Blanco-Gelaz, A. Ferrero-Gutierrez, M. A. Fernandez-Rodriguez, J. Gala and J. Otero-Hernandez, *Transplant. Proc.*, 2013, **45**, 434–439.

2 F. Gaul, W. D. Bugbee, H. R. Hoenecke Jr. and D. D. D'Lima, *Cartilage*, 2018, DOI: 10.1177/1947603518768080.

3 S. Guven, A. Mehrkens, F. Saxer, D. J. Schaefer, R. Martinetti, I. Martin and A. Scherberich, *Biomaterials*, 2011, **32**, 5801–5809.

4 J. N. Harvestine, H. Orbay, J. Y. Chen, D. E. Sahar and J. K. Leach, *J. Mater. Chem. B*, 2018, **6**, 4104–4115.

5 E. J. Lee, F. K. Kasper and A. G. Mikos, *Ann. Biomed. Eng.*, 2014, **42**, 323–337.

6 R. O. Hynes, *Science*, 2009, **326**, 1216–1219.

7 M. Marinkovic, T. J. Block, R. Rakian, Q. Li, E. Wang, M. A. Reilly, D. D. Dean and X. D. Chen, *Matrix Biol.*, 2016, **52**, 426–441.

8 C. D. Reyes, T. A. Petrie and A. J. Garcia, *J. Cell Physiol.*, 2008, **217**, 450–458.

9 J. N. Harvestine, N. L. Vollmer, S. S. Ho, C. A. Zikry, M. A. Lee and J. K. Leach, *Biomacromolecules*, 2016, **17**, 3524–3531.

10 M. L. Decaris, B. Y. Binder, M. A. Soicher, A. Bhat and J. K. Leach, *Tissue Eng., Part A*, 2012, **18**, 2148–2157.

11 A. M. Müller, A. Mehrkens, D. J. Schäfer, C. Jaquiery, S. Güven, M. Lehmicke, R. Martinetti, I. Farhadi, M. Jakob, A. Scherberich and I. Martin, *Eur. Cells Mater.*, 2010, **19**, 127–135.

12 S. Bhumiratana, J. C. Bernhard, D. M. Alfi, K. Yeager, R. E. Eton, J. Bova, F. Shah, J. M. Gimble, M. J. Lopez, S. B. Eisig and G. Vunjak-Novakovic, *Sci. Transl. Med.*, 2016, **8**, 1–13.

13 A. I. Hoch, R. Duhr, N. Di Maggio, A. Mehrkens, M. Jakob and D. Wendt, *Biotechnol. J.*, 2017, **12**, 1700071–1700077.

14 A. Papadimitropoulos, E. Piccinini, S. Brachat, A. Braccini, D. Wendt, A. Barbero, C. Jacobi and I. Martin, *Proc. Natl. Acad. Sci. U. S. A.*, 2014, **9**, 1–12.

15 L. Rödling, I. Schwedhelm, S. Kraus, K. Bieback, J. Hansmann and C. Lee-Thedieck, *Sci. Rep.*, 2017, **7**, 1–15.

16 M. C. Allenby, N. Panoskaltsis, A. Tahlawi, S. B. Dos Santos and A. Mantalaris, *Biomaterials*, 2018, **188**, 24–37.

17 P. E. Bourgine, T. Klein, A. M. Paczulla, T. Shimizu, L. Kunz, K. D. Kokkaliaris, D. L. Coutu, C. Lengerke, R. Skoda, T. Schroeder and I. Martin, *Proc. Natl. Acad. Sci. U. S. A.*, 2018, **115**, E5688–E5695.

18 D. Mitra, J. Whitehead, O. W. Yasui and J. K. Leach, *Biomaterials*, 2017, **146**, 29–39.

19 R. A. Thibault, A. G. Mikos and F. K. Kasper, *Biomacromolecules*, 2011, **12**, 4204–4212.

20 M. L. Decaris, A. Mojadedi, A. Bhat and J. K. Leach, *Acta Biomater.*, 2012, **8**, 744–752.

21 M. L. Decaris and J. K. Leach, *Ann. Biomed. Eng.*, 2011, **39**, 1174–1185.

22 A. I. Hoch, V. Mittal, D. Mitra, N. Vollmer, C. A. Zikry and J. K. Leach, *Biomaterials*, 2016, **74**, 178–187.

23 J. He, D. C. Genetos and J. K. Leach, *Tissue Eng., Part A*, 2010, **16**, 127–137.

24 W. E. Brown, J. C. Hu and K. A. Athanasiou, *Tissue Eng., Part C*, 2016, **22**, 895–903.

25 D. Wendt, A. Marsano, M. Jakob, M. Heberer and I. Martin, *Biotechnol. Bioeng.*, 2003, **84**, 205–214.

26 L. A. Feldkamp, L. C. Davis and J. W. Kress, *J. Opt. Soc. Am. A*, 1984, **1**, 612–619.

27 M. Darnell, S. Young, L. Gu, N. Shah, E. Lippens, J. Weaver, G. Duda and D. Mooney, *Adv. Healthcare Mater.*, 2017, **6**, 1601185–1601192.

28 S. Scaglione, A. Braccini, D. Wendt, C. Jaquiery, F. Beltrame, R. Quarto and I. Martin, *Biotechnol. Bioeng.*, 2006, **93**, 181–187.

29 V. I. Sikavitsas, G. N. Bancroft, H. L. Holtorf, J. A. Jansen and A. G. Mikos, *Proc. Natl. Acad. Sci. U. S. A.*, 2003, **100**, 14683–14688.

30 V. I. Sikavitsas, G. N. Bancroft, J. J. Lemoine, M. A. K. Liebschner, M. Dauner and A. G. Mikos, *Ann. Biomed. Eng.*, 2005, **33**, 63–70.

31 P. Herigou, A. Piognar, F. Beaujean and H. Rouard, *J. Bone Jt. Surg., Am.*, 2005, **87**, 1430–1437.